First neutrino event detection with nuclear emulsion at J-PARC neutrino beamline

Fukuda, T. ; Aoki, S. ; Cao, S. ; Chikuma, N. ; Fukuzawa, Y. ; Gonin, M. ; Hayashino, T. ; Hayato, Y. ; Hiramoto, A. ; Hosomi, F. ; Ishiguro…

(Citation)
Progress of Theoretical and Experimental Physics,2017(6):063C02-063C02

(Issue Date)
2017-06

(Resource Type)
journal article

(Version)
Version of Record

(URL)
https://hdl.handle.net/20.500.14094/90005109

PTEP

Prog. Theor. Exp. Phys. **2017**, 063C02 (23 pages)
DOI: 10.1093/ptep/ptx077

First neutrino event detection with nuclear emulsion at J-PARC neutrino beamline

T. Fukuda[1,*], S. Aoki[2], S. Cao[3], N. Chikuma[4], Y. Fukuzawa[1], M. Gonin[5], T. Hayashino[6], Y. Hayato[7], A. Hiramoto[6], F. Hosomi[4], K. Ishiguro[1], S. Iori[8], T. Inoh[8], H. Kawahara[1], H. Kim[9], N. Kitagawa[1], T. Koga[4], R. Komatani[1], M. Komatsu[1], A. Matsushita[1], S. Mikado[10], A. Minamino[11], H. Mizusawa[8], K. Morishima[1], T. Matsuo[8], T. Matsumoto[8], Y. Morimoto[8], M. Morishita[1], K. Nakamura[6], M. Nakamura[1], Y. Nakamura[1], N. Naganawa[1], T. Nakano[1], T. Nakaya[6], Y. Nakatsuka[1], A. Nishio[1], S. Ogawa[8], H. Oshima[8], B. Quilain[6], H. Rokujo[1], O. Sato[1], Y. Seiya[9], H. Shibuya[8], T. Shiraishi[1], Y. Suzuki[1], S. Tada[1], S. Takahashi[2], K. Yamada[2], M. Yoshimoto[1] and M. Yokoyama[4]

[1]*Nagoya University, Nagoya 464-8601, Japan*
[2]*Kobe University, Kobe 657-8501, Japan*
[3]*High Energy Accelerator Research Organization (KEK), Tsukuba 305-0801, Japan*
[4]*University of Tokyo, Tokyo 113-0033, Japan*
[5]*Ecole Polytechnique, IN2P3-CNRS, Laboratoire Leprince-Ringuet, Palaiseau, France*
[6]*Kyoto University, Kyoto 606-8502, Japan*
[7]*University of Tokyo, ICRR, Kamioka 506-1205, Japan*
[8]*Toho University, Funabashi 274-8510, Japan*
[9]*Osaka City University, Osaka 558-8585, Japan*
[10]*Nihon University, Narashino 274-8501, Japan*
[11]*Yokohama National University, Yokohama 240-0067, Japan*
[*]E-mail: tfukuda@flab.phys.nagoya-u.ac.jp

Received March 13, 2017; Revised May 18, 2017; Accepted May 18, 2017; Published June 30, 2017

Precise neutrino–nucleus interaction measurements in the sub-multi-GeV region are important to reduce the systematic uncertainty in future neutrino oscillation experiments. Furthermore, an excess of ν_e interactions, as a possible interpretation of the existence of a sterile neutrino, has been observed in such an energy region. The nuclear emulsion technique can measure all the final state particles with low energy threshold for a variety of targets (Fe, C, H_2O, and so on). Its sub-μm position resolution allows measurements of the ν_e cross-section with good electron/gamma separation capability. We started a new experiment at J-PARC to study sub-multi-GeV neutrino interactions by introducing the nuclear emulsion technique. The J-PARC T60 experiment has been implemented as a first step in such a project. Systematic neutrino event analysis with full scanning data in the nuclear emulsion detector was performed for the first time. The first neutrino event detection and its analysis are described in this paper.

Subject Index C32

1. Introduction

Currently, many experimental neutrino oscillation projects are running, or planned, to search for CP violation, and/or to probe the neutrino mass hierarchy [1–9]. Precise cross-section measurements of neutrino–nucleus interactions in the sub-multi-GeV region are important to reduce the systematic uncertainty, particularly for the neutrino mixing angle θ_{23}, in these experiments. Furthermore, one possible explanation of the MiniBooNE anomaly [10] in this energy region is a result of the existence

of the so-called sterile neutrino indicated by LSND [11]; precise cross-section measurements are thus also important in verifying the MiniBooNE anomaly.

Nuclear emulsion is a three-dimensional solid tracking detector with sub-micron positional resolution. Thanks to its high spatial resolution, nuclear emulsion technology contributed to the discovery of the pion [12], of the charmed particle in cosmic rays [13], the direct observation of ν_τ [14], the discovery of the ν_τ appearance in a ν_μ beam [15], and so on. This high spatial resolution allows measurements of all the final state particles with a low energy threshold. Nuclear emulsion has 4π track detection capability [16,17]. This is also very useful to investigate the event topology in low-energy neutrino interactions. Furthermore, good e/γ separation capability allows measurement of ν_e charged current interactions with a strong suppression of the background from ν_μ neutral current interactions with π^0 production. There is much flexibility for target material selection because the detector, a so-called emulsion cloud chamber (ECC), is constructed as a sandwich structure of thin nuclear emulsion films and the target materials.

The J-PARC T60 experiment [18,19] was proposed to study the feasibility and check the detector performance of nuclear emulsion at the J-PARC neutrino beamline. The first results of beam exposure in 2015 will be presented in this paper.

Accelerator-based neutrino experiments with nuclear emulsion were established from the end of 1970s [20–22]. The experimental concept is that of a hybrid analysis with the emulsion and the electronic detectors, a so-called "emulsion-counter hybrid experiment." Only a small area of emulsions that is predicted by the electronic detectors has been analyzed, or only a small number of tracks that are predicted have been traced back because of the limitation of the track readout speed in the emulsions. A high-speed scanning system for the emulsion has been developed [23–28], and track readout for the entire area in the emulsion has recently become available. This allows one to analyze the emulsions independently of the prediction from the electronic detectors. In this paper, the first systematic neutrino event analysis from scanning all the data in the nuclear emulsion will also be described.

2. Neutrino detector

2.1. Nuclear emulsion films

The nuclear emulsion gel was produced in the facility at Nagoya University. In this emulsion gel production, high-sensitivity emulsion gel, containing 55% AgBr crystals by volume ratio, was produced [29]. Two emulsion layers, each 50 μm thick, were formed on both faces of a 180 μm-thick polystyrene base. The size of sheets was 100 mm $\times$ 125 mm. The long-term variation of the emulsion sensitivity and background noise was investigated using cut pieces of the emulsion sheets. The emulsion sensitivity was measured as grain density (GD), the number of grains per 100 μm along a minimum ionizing particle (MIP) trajectory. The noise of the emulsion was measured as fog density (FD), the number of randomly distributed grains per 1000 μm^3 in the emulsion. If an emulsion is left undeveloped for a long time after track recording, the silver atoms tend to oxidize into silver ions, owing to the presence of water and oxygen in the material. Some of the latent image cores are destroyed and fewer grains are produced in the development process. This effect is called fading. Variations of GD and FD over 133 days are shown in Fig. 1 under four different temperature and humidity conditions. We found that GD and FD remain at safe levels even after 133 days at 23 °C.

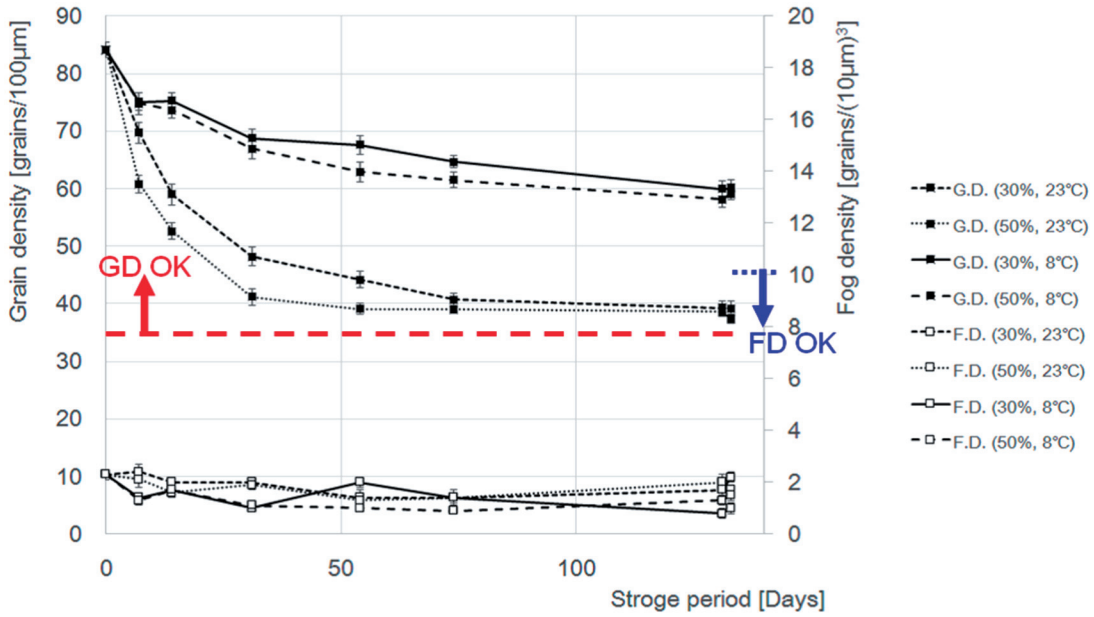

Fig. 1. Initial and long-term performance of emulsion gels. The GD and FD are kept at safe levels (GD $\geq$ 35, FD $\leq$ 10) for 133 days at less than 23 °C. The fading effect is suppressed in low-temperature and low-humidity conditions.

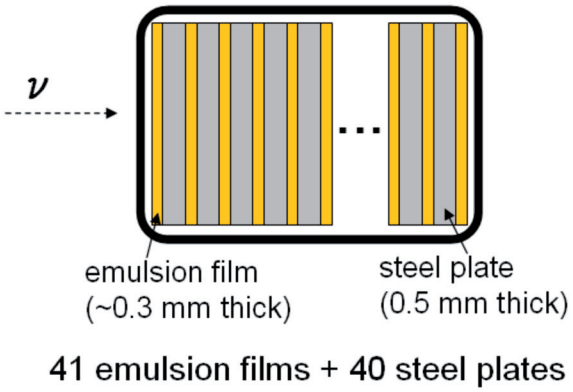

Fig. 2. The emulsion cloud chamber (ECC).

2.2. Emulsion Cloud Chamber

The ECC is constituted by alternatively stacking 41 emulsion films and 40 stainless steel plates (SUS304, 500 μm thickness), as shown in Fig. 2. These are inserted in a paper box and then vacuum-packed with a light-shield aluminum laminated bag in 40% relative humidity conditions. The total target mass is approximately 2.2 kg (1.2 kg inside the fiducial volume).

2.3. Emulsion shifter

Precise tracking detectors with timing information, e.g. a silicon microstrip detector or scintillating fiber detector, have been applied to connect tracks between the main emulsion detector and the electronic detectors, which have muon-identification capability in the conventional emulsion counter hybrid experiment. In the present work, an emulsion device with timing information played

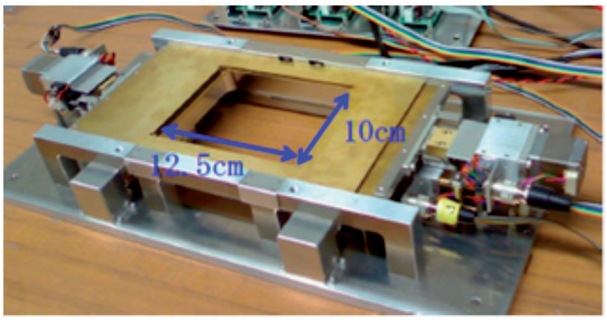

Fig. 3. Emulsion shifter.

this role. The emulsion detector intrinsically has no timing information. Therefore, the timing information is produced from the emulsion tracks by track coincidence between the films on a mechanically controlled moving stage [30,31], the so-called "emulsion shifter." An emulsion shifter (Fig. 3) was reused from a balloon experiment with nuclear emulsion [32]. This equipment gives a time-stamp to the emulsion track by using a clock-based multi-stage emulsion shifter technique. Three stages play the roles of the hour, minute, and second hands of a watch, respectively. Emulsion tracks that are coincident on all three stages obtain a time-stamp corresponding to each stage position. The timing resolution of this emulsion shifter is approximately 7.9 s, which was investigated using tracks passing through the emulsion shifter and electronic detector located at the back of the emulsion detectors. The details for this equipment and the analysis are described in Refs. [32,33].

2.4. Interactive Neutrino Grid (INGRID)

INGRID is one of the near detectors for the T2K experiment [34]. The tracking device is a 1 cm-thickness plastic scintillator (5 cm width) read out with wavelength-shifting fibers. The constitution of the detector is a sandwich structure of the tracking planes and 6.5 cm-thickness iron blocks. The detector was assembled from a total of nine iron layers (58.5 cm) and 11 vertical and horizontal tracking planes. The size of a module is 1.2 m $\times$ 1.2 m $\times$ 0.9 m. INGRID consists of 16 identical modules arranged in horizontal and vertical arrays around the beam center. The original purpose of INGRID was to measure the neutrino beam direction and verify the number of neutrino interactions per protons on target. In the J-PARC T60 experiment, INGRID is utilized to identify the muons from neutrino–nucleus interactions in the ECC. As shown in Fig. 4, the emulsion shifter is placed between the ECC and INGRID. The particles that cross the emulsion shifter are supplied with time-stamps. The tracks are then matched between the emulsion detector and INGRID using the timing information.

2.5. Installation at J-PARC

The emulsion detectors and the assembly frame were prepared at Toho University. These detectors were transported to J-PARC before the installation. The emulsion detectors were installed in front of an INGRID module adjacent to the on-axis module of the Neutrino Monitor Building at J-PARC on 14 January 2015, as shown in Fig. 5. The operation of the emulsion shifter has been monitored by verifying the stage reproducibility, which was sent to Kobe University with a monitoring laptop PC.

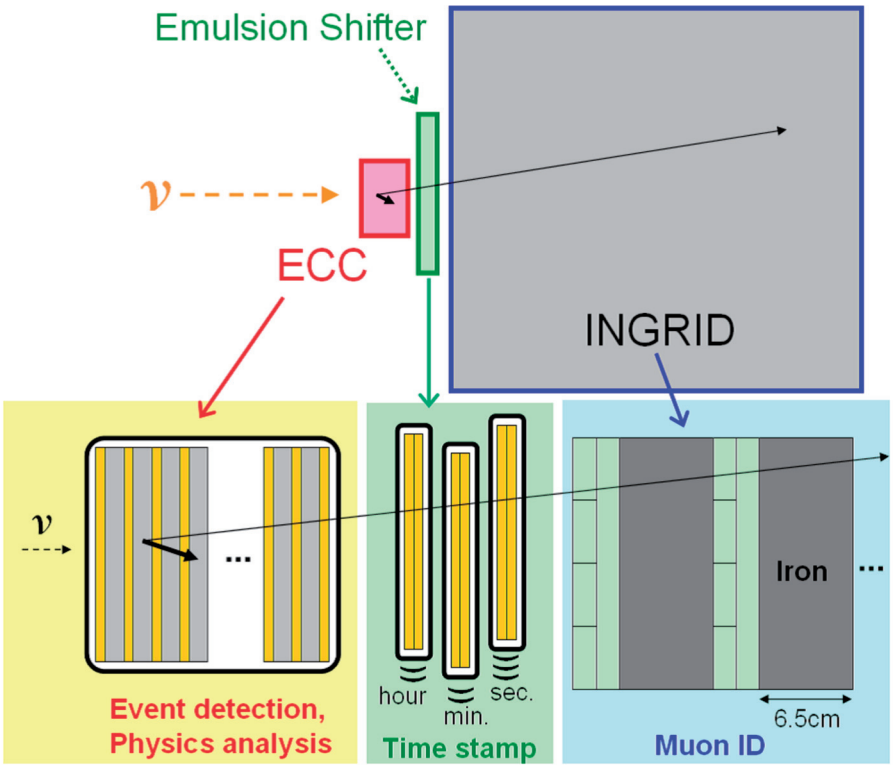

Fig. 4. Detector concept.

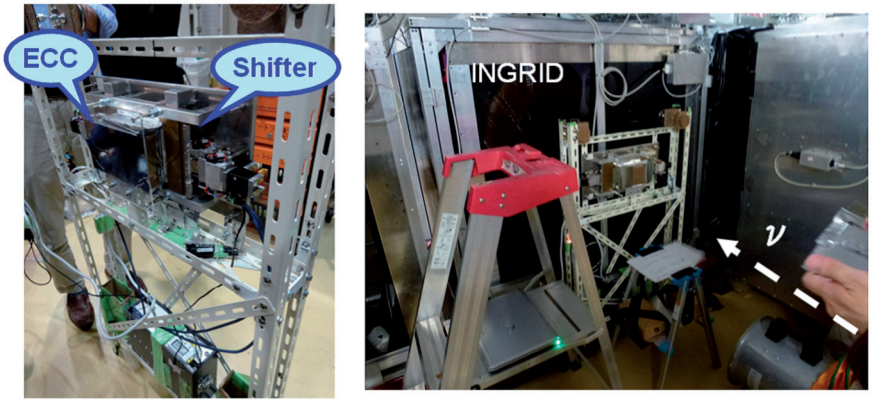

Fig. 5. Detector installation at J-PARC neutrino beamline.

3. Neutrino beam exposure

The neutrino beam exposure started on 15 January 2015. Unfortunately, beam exposure was stopped on 16 January, then restarted from 25 February and finished on 1 April. The beam exposure was performed with the anti-neutrino beam mode after the restart of beam exposure. The accumulated number of protons on target is approximately 13.8×10^{19}. The ratio of neutrino to anti-neutrino interactions is $\sim 1 : 3$ because of the contamination of neutrinos in the anti-neutrino beam. The total number of neutrino or anti-neutrino events is estimated as approximately 44 events (fiducial volume: 24 events, including two events at the region of the emulsion layer). After beam exposure, the stages of the emulsion shifter were moved to a reference position and reference cosmic-ray

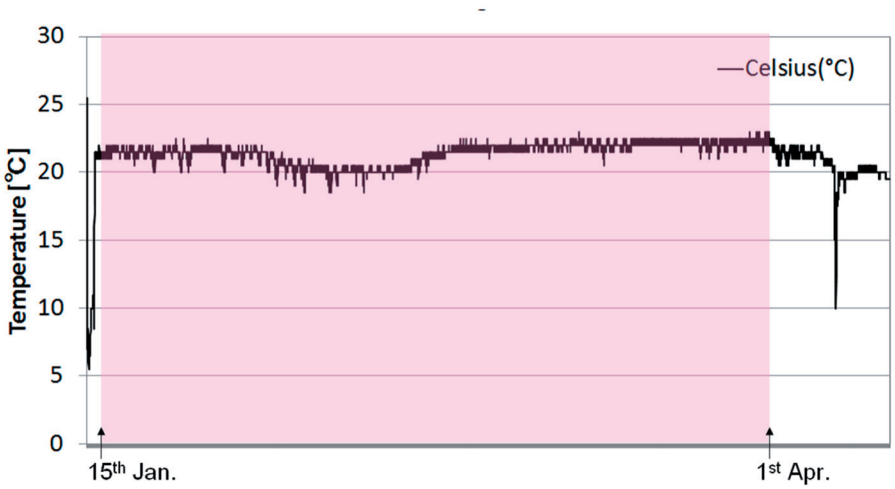

Fig. 6. Temperature at the experimental site.

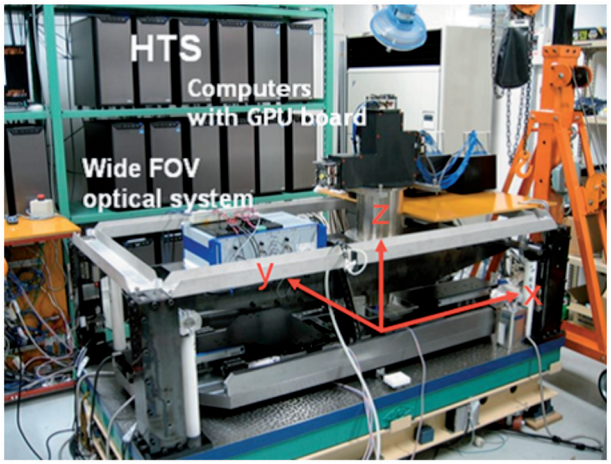

Fig. 7. Hyper Track Selector (HTS).

tracks were accumulated for one week. The emulsion detectors were uninstalled on 8 April and all films were immediately developed at Toho University. The temperature at the experimental site was approximately 22 °C during the exposure, as shown in Fig. 6. Therefore, the tracks that were recorded in the emulsion films were kept in good condition, as shown in Fig. 1. In operation, the emulsion shifter performed well [33].

4. Event analysis

4.1. Scanning

The entire areas of all the emulsion films for the experiment ($\sim$1.2 m^2 for the two emulsion layers of all the emulsion films, including six films for the emulsion shifter) were scanned using a high-speed automated microscope system, Hyper Track Selector (HTS) [28] (Fig. 7). This system was developed at Nagoya University to quickly analyze particle tracks in emulsion films, and allows tracks to be read out at a scanning speed of $\sim$5000 cm^2 h^{-1}. HTS takes 16 tomographic images in an emulsion layer and recognizes a series of grains on a straight line as a track by comparing these images. The

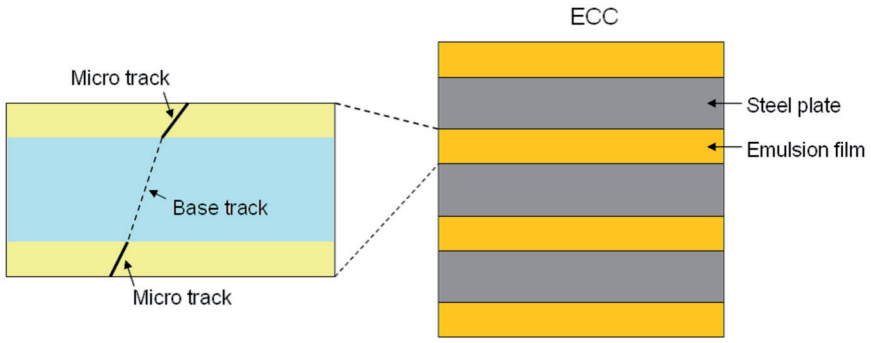

Fig. 8. Schematic view of the track reconstruction in an emulsion film.

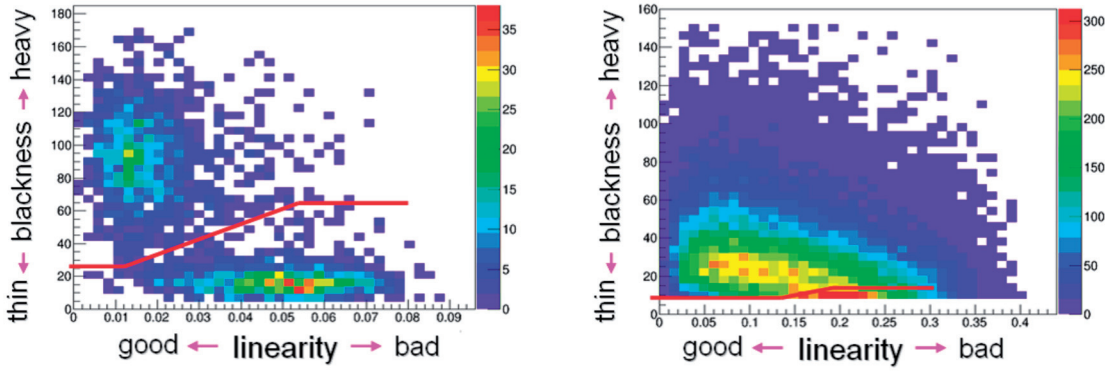

Fig. 9. Track linearity and blackness (left: $|\tan\theta| < 0.1$; right: $|\tan\theta| > 1.4$). The sum of the VPH of micro tracks, which is a reconstructed base track, is shown on the vertical axis. The square root of the sum of squares of the angle difference between the base track and micro tracks is shown on the horizontal axis. The blackness and linearity of fake tracks tend to be thin and bad, respectively. The red line shows the discrimination line and is set for each 100 mrad of track angle.

slope acceptance of HTS was set at $|\tan\theta| < 1.7$ ($|\theta| \lesssim 60°$), where θ is the track angle with respect to the perpendicular of the emulsion film (the z-axis).

4.2. Analysis in ECC

4.2.1. Track reconstruction

First, track segments, so-called "micro tracks," were detected on each layer of the emulsion films (Fig. 8). The positions (x, y), slopes $(\tan\theta_x, \tan\theta_y)$, number of hits in an emulsion layer, pulse height (PH), number of pixels of constructed track data, and volume pulse height (VPH) of the micro tracks were measured by HTS. The number of grains belonging to the track (blackness) is well correlated with the PH and the VPH. As shown in Fig. 8, the tracks connecting the positions of micro tracks on both sides of the plastic base are called "base tracks." Sub-MeV or few-MeV electrons from the environment are recorded in the emulsion because the nuclear emulsion records all tracks from immediately after production until development with no dead time. Therefore, the automated scanning system recognizes "fake" tracks made of low-energy electrons and/or random noise grains (fog). The chance coincidences of these fake tracks become the background of base tracks. However, such background base tracks can be rejected by evaluating their blackness (VPH) and linearity (the angle difference between base track and micro tracks) [35]. Figure 9 shows the blackness versus the linearity of base tracks for a small-angle region ($|\tan\theta| < 0.1$, left panel) and a large-angle

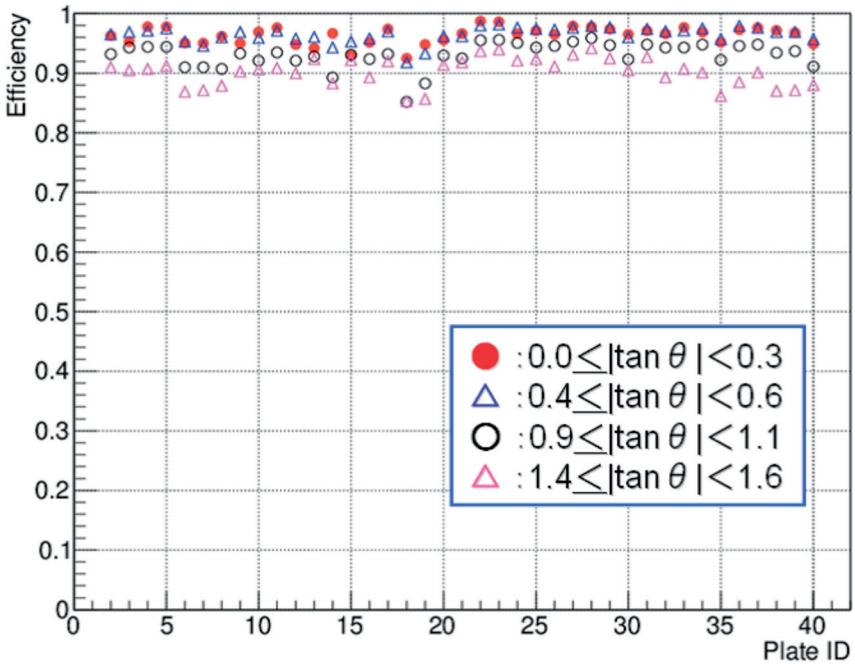

Fig. 10. Track efficiency after reconstruction. When the track efficiency is estimated at one plate, having base tracks at upstream and downstream plates is required to select penetrating tracks in the target plate.

region ($|\tan\theta| > 1.4$, right panel). The VPH and angular accuracy of base tracks depend on their angle. The smaller the track angle, the better the signal-to-noise ratio (S/N) of the base tracks. So the discrimination line is set for each track angle as shown by the red line in Fig. 9. The tracks under the red line are rejected as fake tracks.

The positions (x, y) and slopes ($\tan\theta_x$, $\tan\theta_y$) of the base tracks were measured with respect to the microscope's coordinate system. After connecting the base tracks among the emulsion films, the rotation, slant, parallel translation, and distance between every pair of adjacent emulsion films are adjusted, so that the differences in the track positions and slopes between the two films are minimized after the reconstruction procedure. These connection elements of base tracks are called "linklets." All base tracks in all films are reconstructed by tracking linklets, as a chain. Finally, the track density in a film is $\sim$4000 tracks cm^{-2}. The track efficiency after reconstruction was evaluated at each measured angle for all plates, as shown in Fig. 10. In the small-angle region, the track efficiency is approximately 96%. However, in the large-angle region, the loss of efficiency is visible.

4.2.2. Proton identification

The momentum of charged particles can be estimated in the ECC by measuring their multiple Coulomb scattering (MCS) [36]. When a particle of charge z, momentum p, and velocity βc traverses a material of depth x and radiation length X_0, the deviation of the distribution of the scattering angle is given by:

$$\theta_0 = \frac{13.6\,\mathrm{MeV}}{\beta cp} z \sqrt{\frac{x}{X_0}} \left(1 + 0.038 \ln\left(\frac{x}{X_0}\right)\right). \quad (1)$$

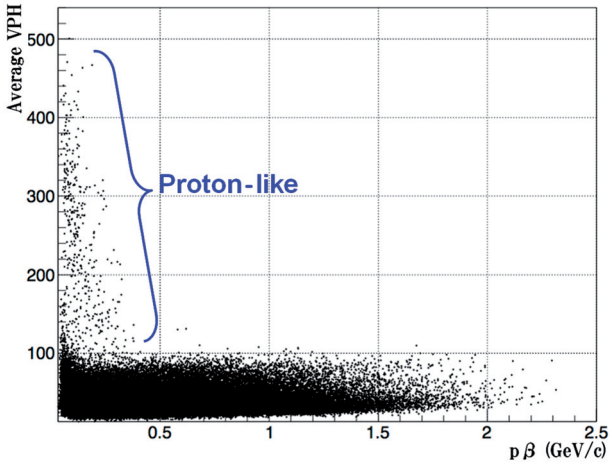

Fig. 11. Proton-like tracks are seen in the low-$p\beta$ and high average VPH region.

The GD is nearly proportional to its energy loss dE/dx in nuclear emulsion [37]. The average number of hit layers (PH) or the average number of pixels associated with the reconstructed track (VPH) in scanned track data corresponds to the GD of tracks [38]. In Fig. 11, the measured momentum and the average VPH of each track that is connected to more than 10 segments is shown. The proton-like tracks are found in the low-momentum and high-dE/dx region.

4.2.3. Track selection

The reconstructed tracks are selected to search for neutrino event vertices as shown in the following steps:

(1) Fiducial area selection: The acceptance of the average track angle is less than $|\tan\theta| = 1.6$ and the searched position area is set at x: 10–120 mm and y: 6–76 mm to avoid the bad film condition area (thin thickness of emulsion layer). The plate IDs of the most upstream and downstream plates in the neutrino beam direction are PL41 and PL01, respectively. The number of tracks and the number of tracks that just start and connect to downstream plates after fiducial selections at each plate are shown in Fig. 12(a). As shown by the red line in Fig. 12(a), there are many tracks upstream of the detector that are identified as penetrating tracks (cosmic ray muons or muons produced from outside of the detector).

(2) Penetrate track veto: Tracks that have at least one segment on three plates at the most upstream position of the ECC (PL41, PL40, PL39) are rejected as penetrate tracks.

(3) Edge out track veto: Tracks are rejected as edge out tracks in the case that the position extrapolated from the most upstream plate to its upstream plate using their position and angle is out of the fiducial area. The number of tracks and the number of starting tracks after veto selections at each plate is shown in Fig. 12(b). The angle distribution of penetrate and edge out tracks is shown in Fig. 13(a). This is consistent with cosmic rays from the sky. Figure 13(b) shows the track angle distribution after (1)–(3) selections. Low-energy tracks or electron/positron pairs from gamma-rays or low-efficiency tails from large-angle tracks still remain as background for starting tracks in the ECC.

(4) Final track selection for vertex search: The tracks that have at least three segments and for which the track angle is less than $|\tan\theta| = 1.5$ ($|\theta| \sim 56°$) at the most upstream plate are

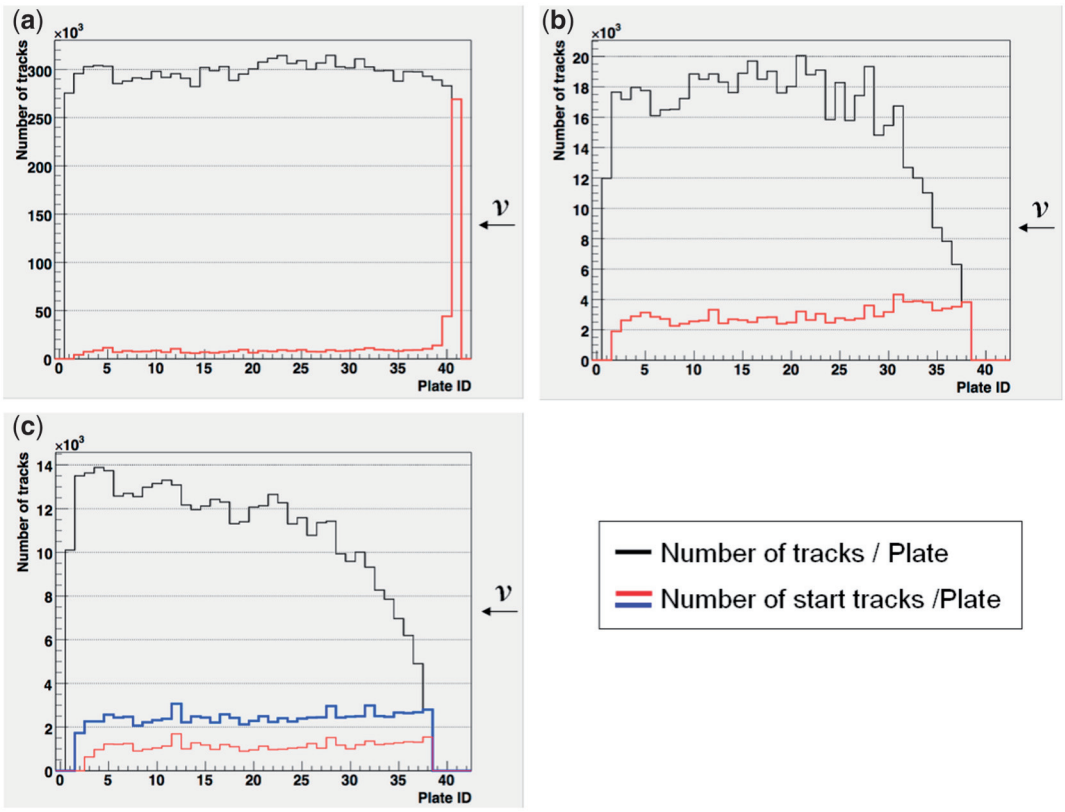

Fig. 12. (a): Number of tracks (black) and starting tracks (red) at each plate after fiducial selections. (b): Number of tracks (black) and starting tracks (red) at each plate after veto selections. (c): Number of tracks (black), number of starting tracks (blue), and number of starting tracks that have at least three segments (red) at each plate after final track selection.

selected to avoid accidentally disconnecting tracks in the large-angle region and low reliability tracks. Finally, 41087 tracks are selected as the candidate tracks from neutrino interactions. The number of tracks and the number of starting tracks after these selections at each plate are shown in Fig. 12(c). Additionally, the track angle distribution after this selection is shown in Fig. 13(c).

4.2.4. Event selection

The event selection is performed with the following procedure. The events are then categorized into types (a)–(h), as shown in Fig. 14.

(1) Vertex search: The most upstream base tracks converge at a point within a 3 σ position difference that is calculated from their angular accuracy and the MCS, assuming a momentum of 400 MeV/c. For example, the position allowance for the minimum distance between two tracks ($\tan\theta = 0.5$, respectively) is approximately 20 μm at the level of 500 μm of iron above the surface of the emulsion film. In this search, the tracks that emit to the forward direction are selected as vertex tracks.

Most of the starting tracks are accidental disconnecting tracks or stopped cosmic-ray tracks from the back of the ECC. So the positions of these tracks are random and fake vertices are created with their accidental chance coincidence. Such background vertices can be emulated by shuffling

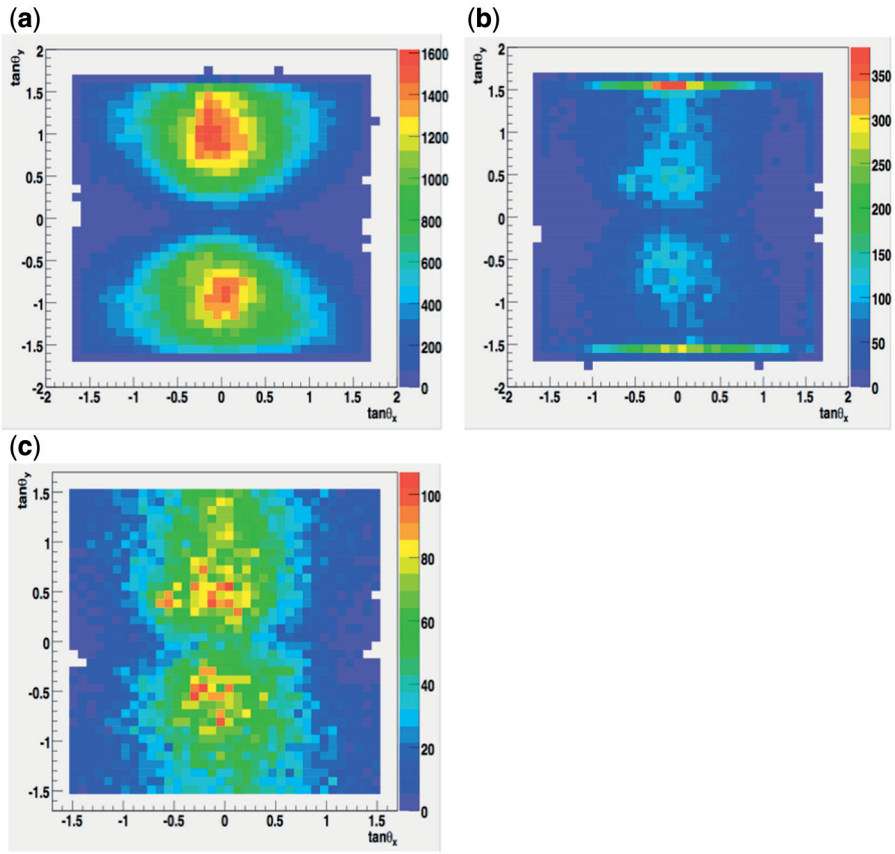

Fig. 13. (a): Angle distribution of penetrate and edge out tracks. (b): Angle distribution of remaining tracks after penetrate and edge out track cut. (c): Angle distribution of finally selected tracks for neutrino event search.

only track positions randomly in each plate and making vertices. Repeating this procedure 10 times, the background number is estimated as the average value in Fig. 14.

(2) Track multiplicity: As a first step, reconstructed vertices are categorized based on their track multiplicity. The three categories are "three and more tracks," "two tracks," and "single track." "Three and more tracks" are categorized as Category (a).
In Category (a), 7 vertices composed of 25 tracks are found and the estimated number of background vertices is less than 0.1. Thus, the vertices of Category (a) are real vertex candidates because of the low background. In the two-track vertex category, there are 269 vertices composed of 537 tracks, including one duplicated case, as shown in Fig. 15, corresponding to 112.6 background vertices. Then, 40525 tracks are categorized as "single track" vertex events [Category (c)]. Single track vertices are mainly considered to be disconnecting of low-energy cosmic ray muons or from electron/positron pair production, as shown in Fig. 13(c).

(3) Track blackness: "Two track" vertices are categorized according to track blackness. Black tracks are defined as tracks whose average VPH is over 120, and minimum ionizing particle (MIP) tracks are defined as tracks whose average VPH is less than 120, as shown in Fig. 11. When two-track vertices are reconstructed by only black tracks, they belong to Category (b). In Category (b), 18 vertices composed of 36 tracks are found, corresponding to 0.5 background vertices. Thus, they are also real vertex candidates. When one black track and one MIP track made a vertex, there are 20 vertices with 40 tracks and the number of the estimated background is 10.8.

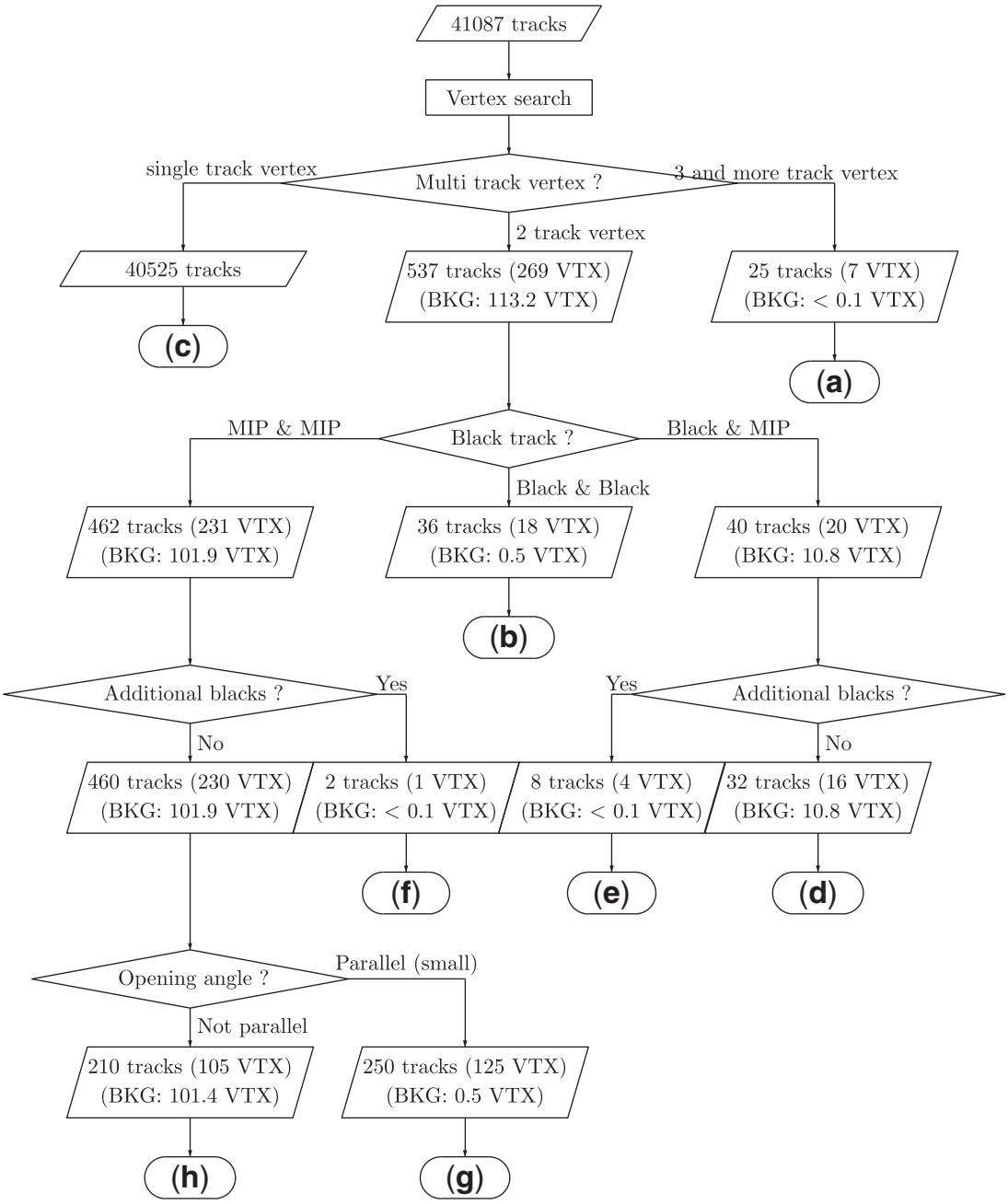

Fig. 14. Flow chart for event selection.

(4) Additional black search: The short black tracks made by only one or two plates are added as vertex tracks. This procedure is done for short black tracks in both forward and backward directions. When short black tracks are sought, around 20 vertices that are reconstructed by one black track and one MIP track, four new vertices with multiple black tracks are found with less than 0.1 background [Category (e)]. Other vertices are stored in Category (d). Also attached to additional black tracks are 231 two-track vertices that are reconstructed by only MIPs. One new vertex with two MIPs and one short black track is found. These vertices are stored in Category (f).

(5) Track parallelness: Figure 16(a) shows the opening angle of 230 MIP vertices with no additional black tracks. The opening angle of ten times of background data is shown in Fig. 16(b).

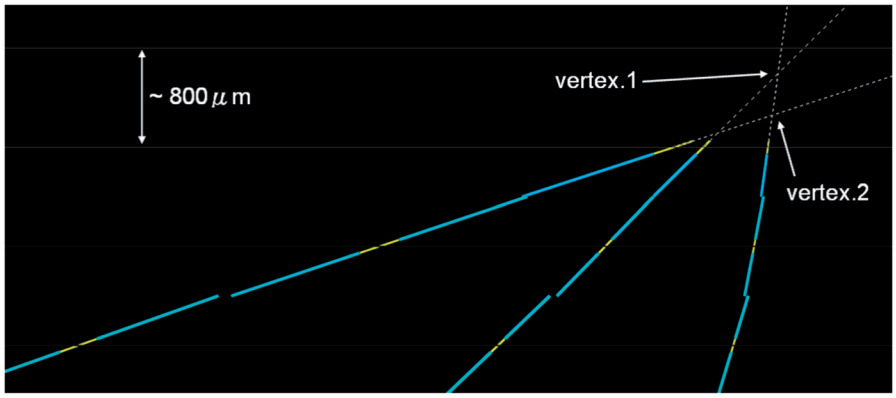

Fig. 15. Two vertices are reconstructed by three tracks.

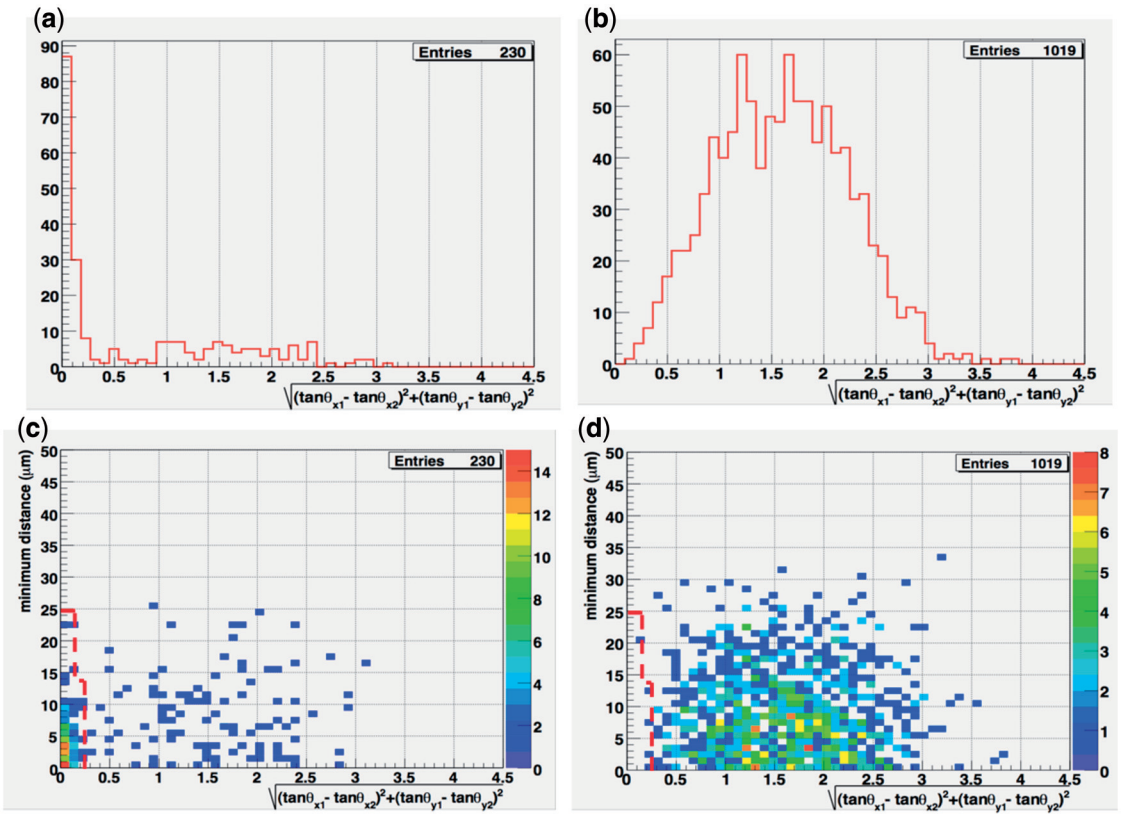

Fig. 16. Opening angle between two tracks in real data (a) and 10 times the estimated background data (b). The opening angle vs. minimum distance between two tracks in real data (c) and 10 times the estimated background data (d). Gamma-ray events are selected within the dotted red line in (c) and (d).

According to the comparison between real and background data, an excess of small opening angle is found in the real data. They are almost parallel tracks, so are explained as electron/positron pair production from gamma-rays. Gamma-ray candidate events are selected by using their opening angle and minimum distance of vertex tracks as shown in Fig. 16(c). Thus, 125 vertices are selected as gamma-ray events and the estimated number of background is 0.5, as shown in Fig. 16(d). Gamma-ray events are stored in Category (g), and the other vertices are stored in Category (h).

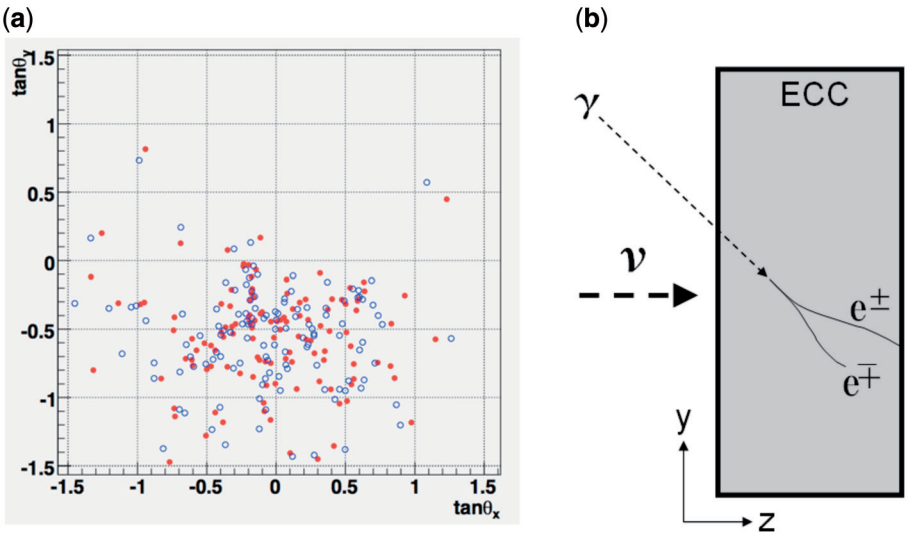

Fig. 17. Angle distribution of electron/positron pairs (red or blue) from gamma-rays.

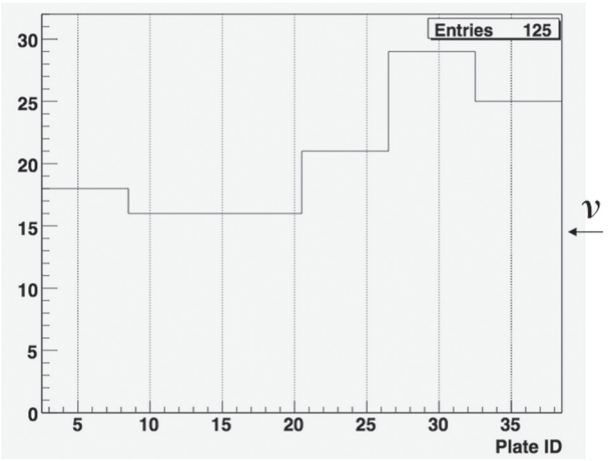

Fig. 18. Converted plate distribution of gamma-rays.

Through the event selections, Categories (a), (b), (e), (f), and (g) are selected as vertex events with high reliability. The 125 events in Category (g) are gamma-ray candidates because they have no black track and their opening angle is small. The 18 vertices in Category (b) are reconstructed by only black tracks, so it is considered that these events are from neutron interactions or part of neutrino neutral current interactions. The neutrino candidate events are stored in Categories (a), (e), and (f). The 12 vertices in these categories have some MIP and black tracks.

On the other hand, there may be some neutrino events in Category (d) because the number of vertex signals is 5.2 ($= 16 - 10.8$). The near vertices in Category (h) are accidental chance coincidence of misconnected cosmic-ray muons or from an electron/positron pair. It is considered that they are the same group as Category (c).

4.3. Gamma-ray events

In this section, Category (g), or gamma-ray candidate events, will be discussed. Only forward-going gamma-rays are reconstructed in this category. The angle distribution of gamma-ray candidate events

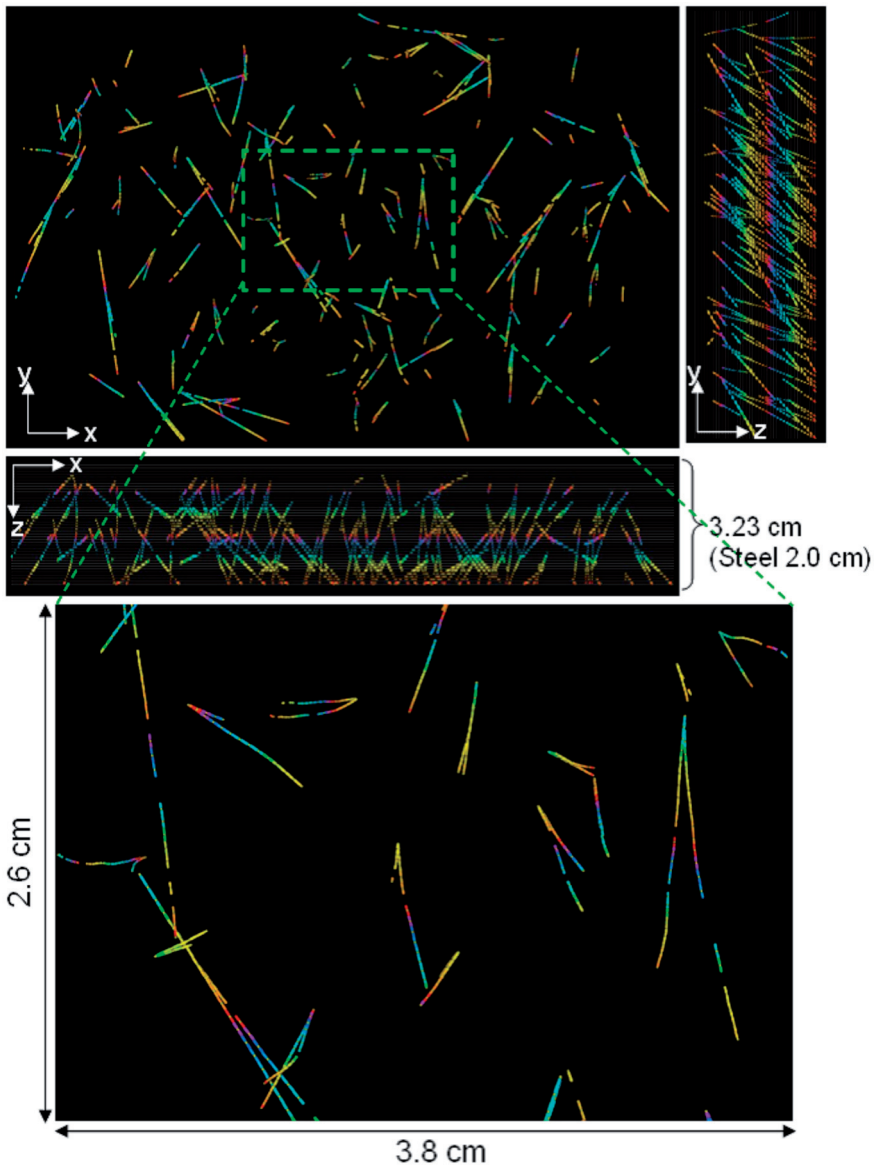

Fig. 19. Three-dimensional (x–y, x–z, y–z) and zooming view. Neutrino beam direction is the same as the z-axis.

is shown in Fig. 17(a). The incident direction of tracks from gamma-rays is the forward and upper side, and it is consistent with the direction of cosmic-rays [Fig. 17(b)]. Additionally, the number of converted gamma-rays is high in the upstream region of the detector, as shown in Fig. 18. This is evidence that the gamma-rays come from outside the detector. The detected electron/positron pairs from gamma-rays in the ECC are shown in Fig. 19. It is considered that cosmic gamma-rays from the backward and upper side directions make the single-track vertex in Category (c) and background vertices.

4.4. Black track vertex events

In this section, a discussion of the 18 vertices found that are reconstructed by only black tracks in Category (b) will be presented. The chance coincidence background is estimated as 0.5 events. Therefore, almost all the events are real vertices. These events are considered as neutron interactions

Table 1. Black track vertices.

2 track vertex	3 track vertex	4 track vertex
7	8	3

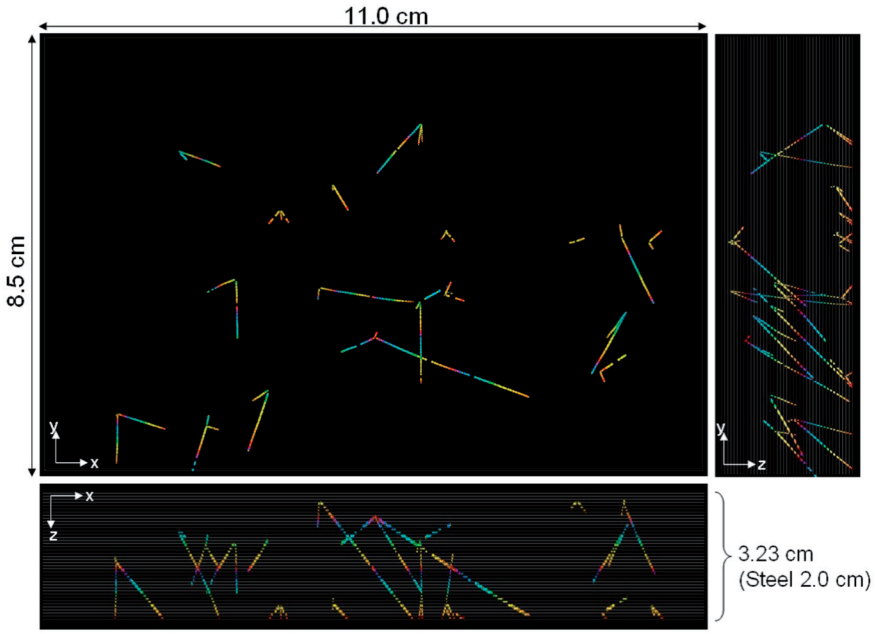

Fig. 20. Three-dimensional view of black vertex events. Neutrino beam direction is parallel to the z-axis.

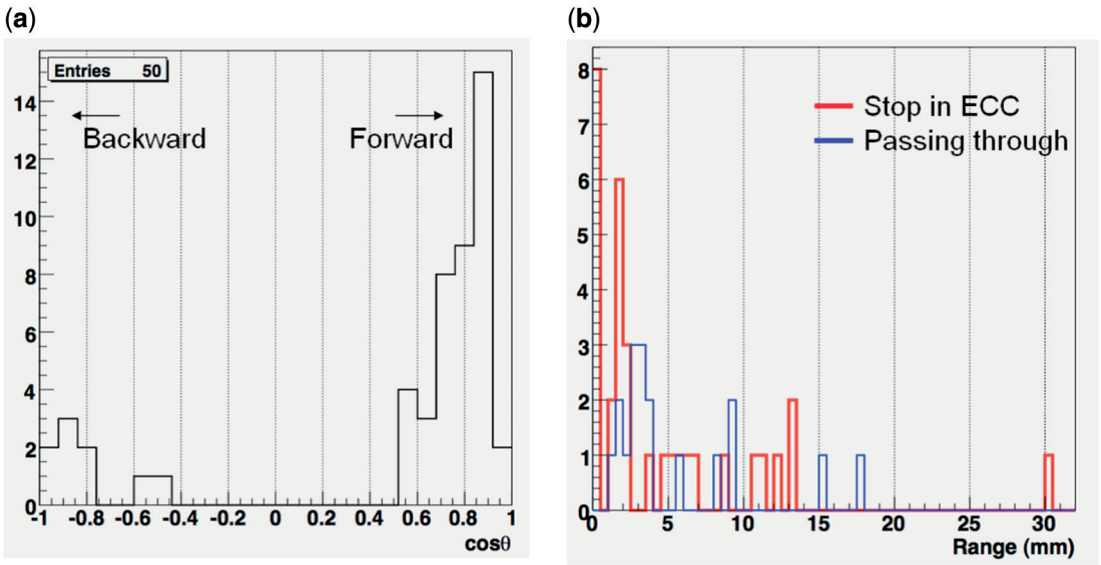

Fig. 21. Emission angle distribution (a) and the range distribution (b) of tracks in black vertex events.

or part of neutrino neutral current interactions with no MIP tracks. Additional short or backward black tracks attached to these vertices were also searched for. As shown in Table 1, new black tracks were found in more than half of the events. The event feature is shown in Fig. 20. The emission angle and range distributions are shown in Fig. 21(a) and (b), respectively. Under the current selection

Table 2. Event summary.

Event number	VTX plate	Material	Multiplicity (MIP)	Multiplicity (Black)	Multiplicity (e^+e^-)
1	8	iron	5	0	3
2	13	iron	2	1	0
3	14	iron	3	2	0
4	23	iron	2	2	0
5	26	iron	1	7	0
6	26	iron	1	3	1
7	27	emulsion	2	2	1
8	28	emulsion	3	7	0
9	30	iron	1	2	0
10	31	iron	1	2	1
11	33	iron	2	2	1
12	36	iron	1	2	0

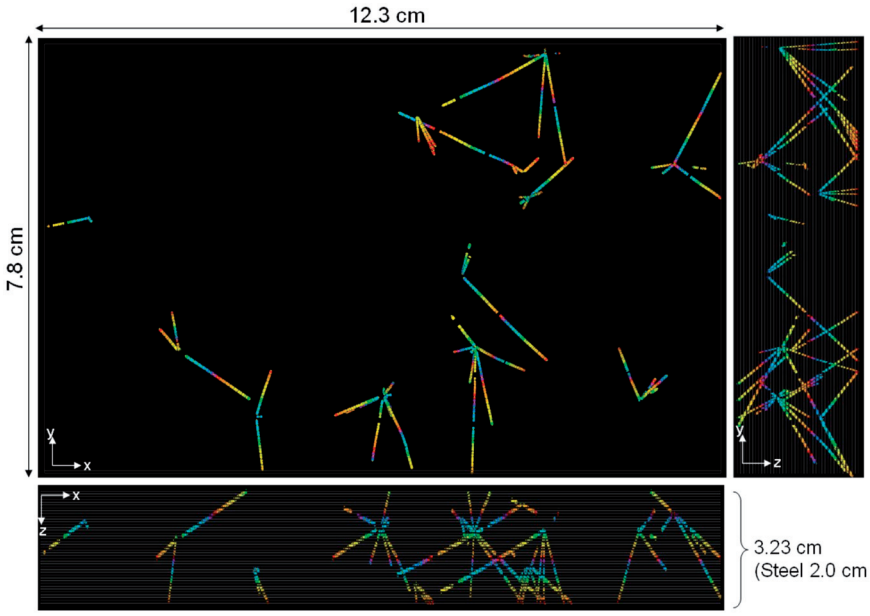

Fig. 22. Three-dimensional view of neutrino candidate events. The neutrino beam direction is parallel to the z-axis.

criteria, the existence of two black tracks that are emitted to the forward direction is required. Thus, this becomes one of the biases to drop neutron events from the backward direction.

4.5. Neutrino candidate events

The other converged tracks, for example low-energy tracks, tracks emitted to the backward direction, or electron/positron pairs from vertices, are searched for in the 12 vertices found in Categories (a), (e), and (f). The detected particle momenta are then measured with MCS and the timing information is obtained with the emulsion shifter to connect the INGRID and identify muons [33]. In this section, the event summary is shown in Table 2 and then some of the detailed event features are described.

The position distribution of 12 vertices is shown in Fig. 22. The impact parameter (IP) and emission angle for each MIP and black tracks is also shown in Fig. 23.

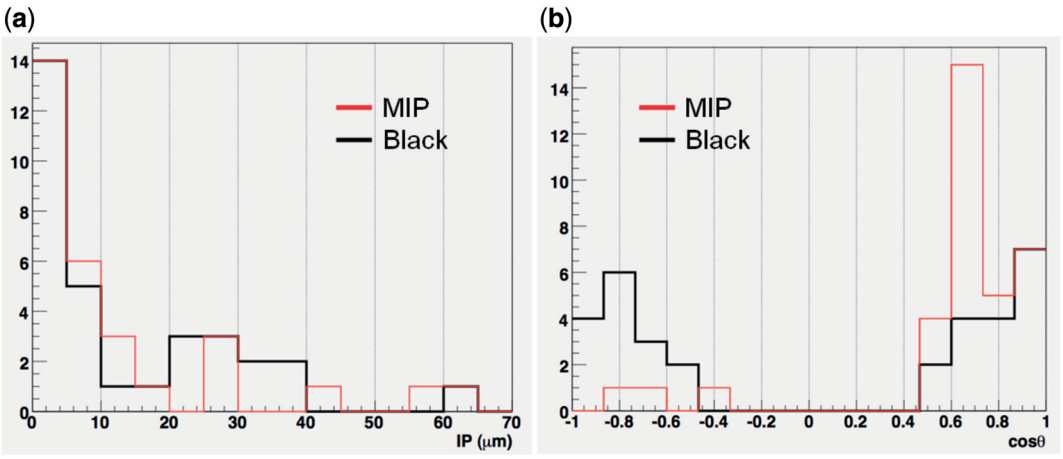

Fig. 23. Impact parameter and emission angle for MIP and black tracks.

Table 3. Track information for Event 7.

PL	Segment ID	$\tan\theta_x$	$\tan\theta_y$	Impact parameter (μm)	PH_{av}	VPH_{av}	$p\beta$ (GeV/c)	PID
27	608427	0.2064	−1.0459	0.7	29.5	182.8	$0.43^{+0.07}_{-0.07}$	proton
27	608429	−0.0661	−0.7599	0.6	27.7	122.3	$0.46^{+0.07}_{-0.07}$	proton
27	608428	−0.0059	0.0540	0.7	30.2	118.3	$4.00^{+\infty}_{-1.75}$	muon
27	608433	−0.9756	−0.5322	0.9	24.7	60.8	$0.21^{+0.03}_{-0.03}$	MIP
21	586893	−0.2365	−0.0407	29.3	27.9	70.0	$0.21^{+0.02}_{-0.03}$	$e^{\pm}$
21	586883	−0.2190	−0.0666	159.3	27.7	72.1	$0.08^{+0.02}_{-0.02}$	$e^{\mp}$

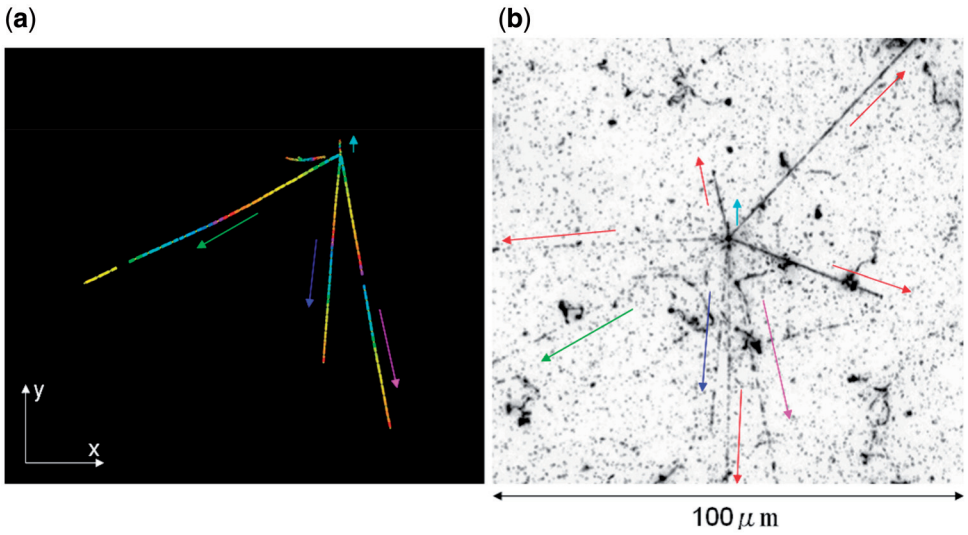

Fig. 24. Event 7.

4.5.1. Event 7

The vertex is in the emulsion region at plate 27 and its vertex point is $(x, y) = (96034.4\,\mu\text{m}, 74184.9\,\mu\text{m})$ in the ECC coordinate system (the origin (0.0 μm, 0.0 μm) is the corner at PL01). One electron/positron pair from a gamma-ray in Category (g) points to this vertex point. The detailed track information is listed in Table 3. There are two MIP tracks and two black tracks in the vertex [Fig. 24(a)]. Also, this event was created at the emulsion region, so we could see more detail

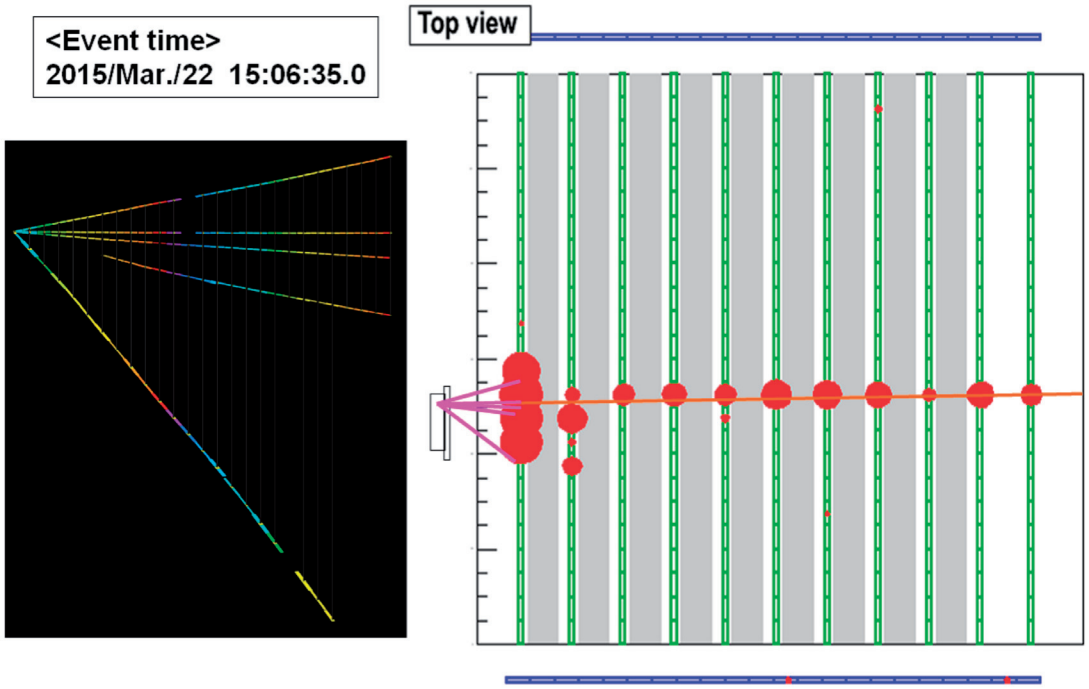

Fig. 25. Event 7: Hybrid analysis with INGRID (top view).

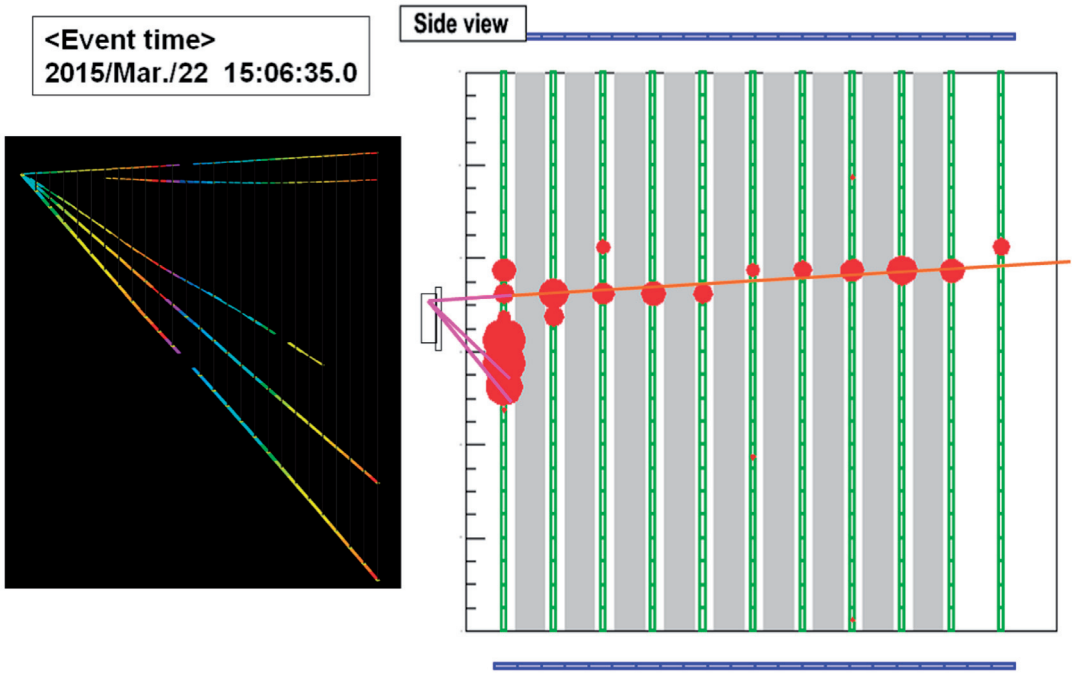

Fig. 26. Event 7: Hybrid analysis with INGRID (side view).

with a microscope. As shown in Fig. 24(b), additional very large angle tracks and black tracks, shown as red arrows, were observed. Additionally, this event was given a time-stamp by analyzing the emulsion shifter, then the timing matching between the emulsion detector and INGRID succeeded uniquely. As shown in Figs. 25 and 26, a muon track is found and the event feature is well matched. Furthermore, the measured track momenta in ECC are consistent with the measured track

Table 4. Track information for Event 3.

PL	Segment ID	$\tan\theta_x$	$\tan\theta_y$	IP (μm)	PH_{av}	VPH_{av}	$p\beta$ (GeV/c)	PID
14	312320	−0.1029	−0.2115	4.8	26.5	62.6	$2.21^{+5.42}_{-0.83}$	muon/pion
14	312317	−0.1830	−0.0077	4.9	27.1	63.2	$1.09^{+0.36}_{-0.25}$	pion/muon
14	312315	0.2550	0.1005	0.4	31.1	150.6	$0.27^{+0.06}_{-0.06}$	proton
14	297419	0.7655	0.6744	9.3	23.1	39.1	$0.30^{+0.06}_{-0.06}$	MIP
13	328835	−0.3979	−0.2846	57.8	24.3	49.0	—	$e^{\pm}$

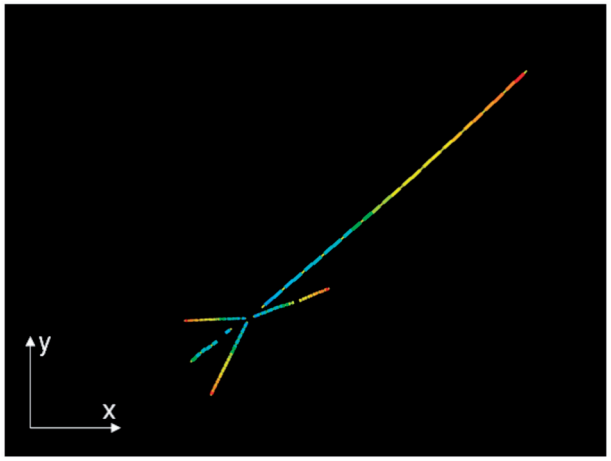

Fig. 27. Event 3.

ranges in INGRID. The momentum of the muon candidate track is also enough to pass through INGRID.

4.5.2. Event 3

The vertex is the steel region upstream of plate 14, and its vertex point is $(x, y) = (93105.6\,\mu\text{m}, 48182.9\,\mu\text{m})$ in the ECC coordinate system. There are three MIP tracks and one black track at the vertex. The details of the event tracks are listed in Table 4. This event is also matched between the emulsion detector and INGRID with the timing information, as shown in Figs. 28 and 29. The measured track momenta are consistent with the measured range in INGRID. Unfortunately, since two tracks penetrate through INGRID, it is difficult to decide which is the muon track from the information from INGRID.

5. Future prospects

5.1. Improvement of the systematic analysis

Further neutrino events are going to be searched for in Categories (c), (d), and (h). It is important to reject many fake starting tracks to find new neutrino events. To do that, the energy threshold to connect tracks between emulsion films will be lowered. Another method is to reconstruct the electron/positron pairs of gamma-rays and neutron-interacted vertices from the backward direction. Then, the search for additional much larger-angle black tracks will also be effective in identifying the interaction point with large-angle track scanning [16,17]. Furthermore, when some tracks reach the emulsion shifter, it will be possible to take the coincidence with timing information for background rejection.

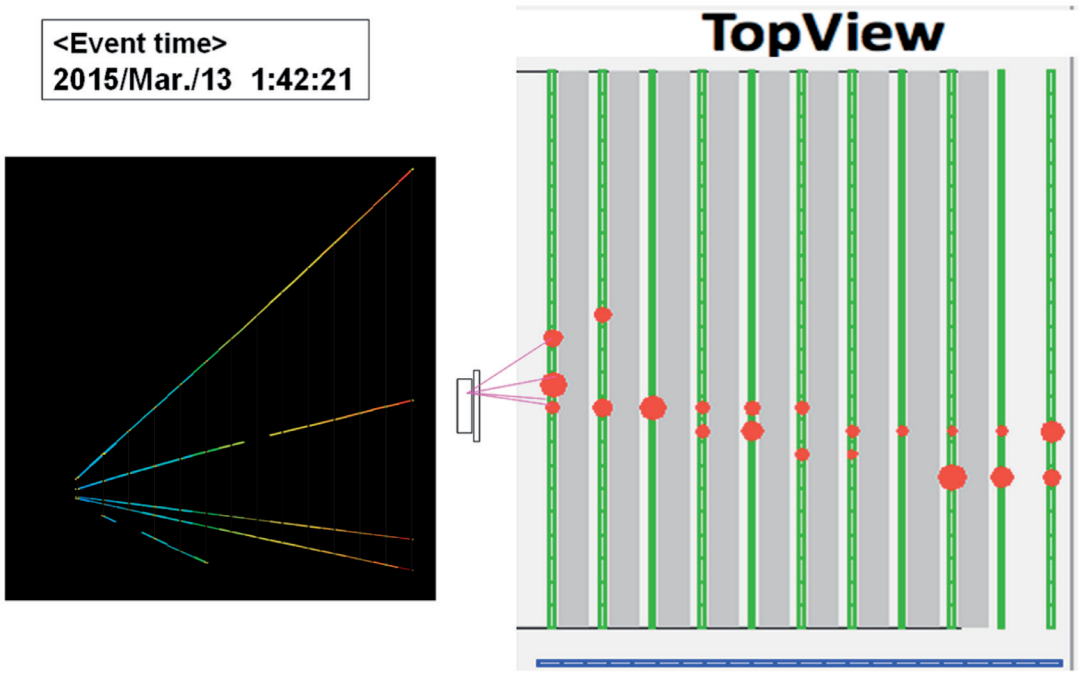

Fig. 28. Event 3: Hybrid analysis with INGRID (top view).

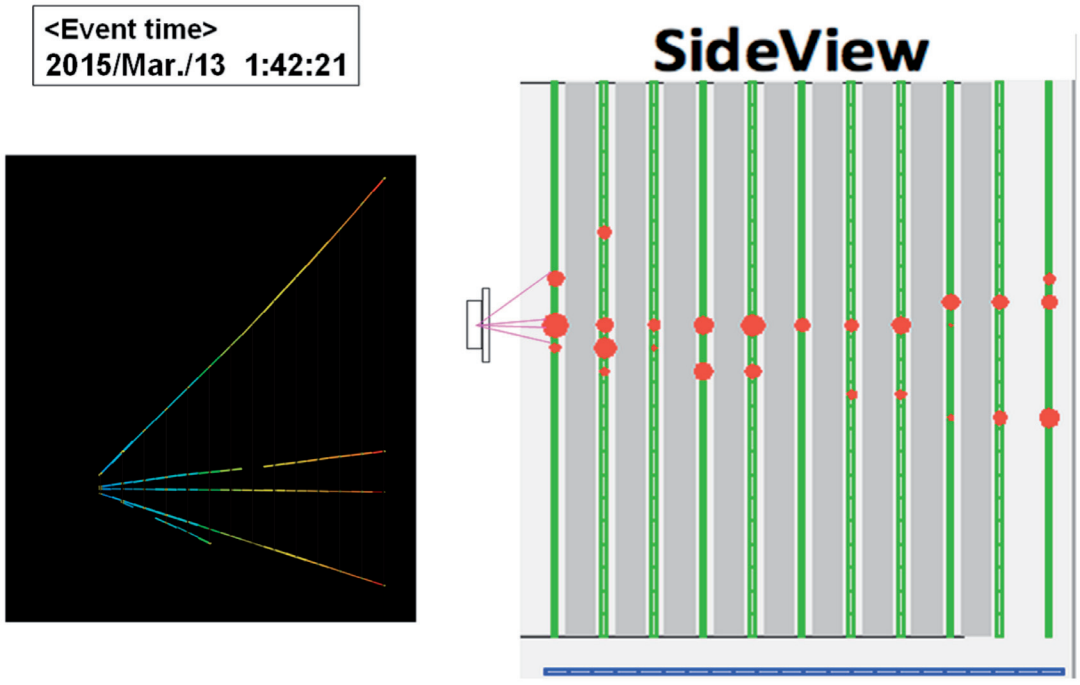

Fig. 29. Event 3: Hybrid analysis with INGRID (side view).

5.2. Future experimental plan

In 2016, an anti-neutrino beam was exposed to a 60 kg steel target, and ECC and film scanning was done. Currently, the neutrino event analysis for this experiment is in progress to investigate the detector performance with higher statistics. Approximately 3000 anti-neutrino interaction events are

expected to accumulate in this ECC. Moreover, not only anti-muon neutrino events but also anti-electron neutrino events will be detected. Furthermore, the neutrino analysis will proceed in a few-kg water-target emulsion chamber that is assembled with vacuum-packed emulsion films and frame-type spacers to fill the water as a target. The status and results of these analyses will be reported in the future. Then, a large-scale water-target emulsion chamber will be constructed to study the neutrino–water interactions in detail.

6. Conclusion

We proposed a new experimental project with a nuclear emulsion detector to study low-energy neutrino–nucleus interactions in detail for future neutrino oscillation physics experiments. The J-PARC T60 experiment has been implemented as a first step in this program to check the feasibility and confirm the neutrino event analysis. In this work, systematic neutrino event analysis with full ECC scanning data has been developed, and the first neutrino event detection has been successfully demonstrated. Moreover, hybrid analysis with INGRID has been performed for the first time. We will polish the systematic neutrino analysis chain, develop the water-target emulsion chamber, and steadily expand the detector scale to reach the desired physics output.

Acknowledgements

We appreciate the support provided by the J-PARC Neutrino Group / Accelerator Group and the T2K Collaboration. We acknowledge support from the Japan Society for the Promotion of Science (JSPS) through their grants (JSPS KAKENHI Grant Numbers 25105001, 25105006, 26105516, 26287049, 25707019, 20244031, 26800138, 16H00873).

Funding

Open Access funding: SCOAP[3].

References

[1] K. Abe et al. [T2K Collaboration], Phys. Rev. D **88**, 032002 (2013).
[2] K. Abe et al. [Hyper-Kamiokande Proto-Collaboration], Prog. Theor. Exp. Phys. **2015**, 053C02 (2015).
[3] P. Adamson et al. [NOvA Collaboration], Phys. Rev. Lett. **116**, 151806 (2016).
[4] R. Acciarri at al. [DUNE Collaboration], arXiv:1512.06148 [physics.ins-det] [Search INSPIRE].
[5] F. An et al. [JUNO Collaboration], arXiv:1507.05613 [physics.ins-det] [Search INSPIRE].
[6] S. B. Kim, arXiv:1504.08268 [physics.ins-det] [Search INSPIRE].
[7] M. Athar et al. [INO Collaboration], *India-Based Neutrino Observatory Project Report* (available at http://www.imsc.res.in/∼ino/OpenReports/INOReport.pdf, date last accessed 25 May, 2016).
[8] M. G. Aartsen et al. [IceCube PINGU Collaboration], arXiv:1401.2046 [physics.ins-det] [Search INSPIRE].
[9] S. Adrian-Martinez et al. [KM3NeT Collaboration], arXiv:1601.07459 [astro-ph.IM] [Search INSPIRE].
[10] A. A. Aguilar-Arevalo et al. [MiniBooNE Collaboration], Phys. Rev. Lett. **110**, 161801 (2013).
[11] A. Aguilar et al. [LSND Collaboration], Phys. Rev. D **64**, 112007 (2001).
[12] C. M. G. Lattes, H. Muirhead, G. P. S. Occhialini, and C. F. Powell, Nature **159**, 694 (1947).
[13] K. Niu, E. Mikumo, and Y. Maeda, Prog. Theor. Phys. **46**, 1644 (1971).
[14] K. Kodama et al. [DONUT Collaboration], Phys. Lett. B **504**, 218 (2001).
[15] N. Agafonova et al. [OPERA Collaboration], Phys. Rev. Lett. **115**, 121802 (2015).
[16] T. Fukuda, S. Fukunaga, H. Ishida, K. Kodama, T. Matsuo, S. Mikado, S. Ogawa, H. Shibuya, and J. Sudo, JINST **8**, P01023 (2013).
[17] T. Fukuda et al., JINST **9**, P12017 (2014).
[18] S. Aoki et al., KEK/J-PARC-PAC 2014-17, (2014).
[19] S. Aoki et al., JPS Conf. Proc. **8**, 023004 (2015).

[20] A. L. Lead et al., Phys. Rev. D **19**, 1287 (1979).
[21] N. Ushida et al. [Fermilab E531 Collaboration], Nucl. Instrum. Meth. A **224**, 50 (1984).
[22] E. Eskut et al. [CHORUS Collaboration], Nucl. Instrum. Meth. A **401**, 7 (1997).
[23] K. Niwa, K. Hoshino, and K. Niu, Proc. Int. Cosmic Ray Symp. High Energy Phenomena, Tokyo, p. 149 (1974).
[24] S. Aoki, K. Hoshino, M. Nakamura, K. Niu, K. Niwa, and N. Torii, Nucl. Instrum. Meth. B **51**, 466 (1990).
[25] T. Nakano, Ph.D. Thesis, Nagoya University, Japan, 1997 (in Japanese).
[26] T. Nakano and K. Morishima, J. SPSTJ. **72**, 229 (2008).
[27] K. Morishima and T. Nakano, JINST **5**, P04011 (2010).
[28] M. Yoshimoto, T. Nakano, R. Komatani. and H. Kawahara, arXiv:1704.06814 [physics.ins-det] [Search INSPIRE].
[29] N. Naganawa and K. Kuwabara, Abstract for SPIJ's annual conference (2011) (in Japanese).
[30] K. Kodama et al., Advances in Space Research **37**, 2120 (2006).
[31] S. Takahashi et al., Nucl. Instrum. Meth. A **620**, 192 (2010).
[32] H. Rokujo et al., Nucl. Instrum. Meth. A **701**, 127 (2013).
[33] K. Yamada et al. [J-PARC T60 Collaboration], arXiv:1703.037037 [physics.ins-det] [Search INSPIRE].
[34] K. Abe et al. [T2K Collaboration], Nucl. Instrum. Meth. A **694**, 211 (2012).
[35] T. Fukuda, K. Kodama, M. Komatsu, S. Miyamoto, K. Morishima, T. Nakano, T. Omura, Y. Sakatani, and O. Sato, JINST **5**, P04009 (2010).
[36] N. Agafonova et al. [OPERA Collaboration], New J. Phys. **14**, 013026 (2012).
[37] T. Fukuda, OPERA Public Note, No. 179 (2015) (available at: http://operaweb.lngs.infn.it/Opera/publicnotes/OPERA_note_179.pdf, date last accessed May 25, 2017).
[38] T. Toshito, A. Ariga, T. Ban, K. Hoshino, M. Komatsu, N. Naganawa, M. Nakamura, T. Nakano, and K. Niwa, Nucl. Instrum. Meth. A **516**, 436 (2004).